Weather and Climate Extremes 52 (2026) 100895

Contents lists available at ScienceDirect

Weather and Climate Extremes

journal homepage: www.elsevier.com/locate/wace

Intrinsic predictability of heavy precipitation influenced by atmospheric rivers in the Western Iberian Peninsula

Ehud Bartfeld [a,*,1], Alexandre M. Ramos [b,1], Assaf Hochman [a,1]

[a] Fredy and Nadine Herrmann Institute of Earth Sciences, The Hebrew University of Jerusalem, Jerusalem, Israel
[b] Institute of Meteorology and Climate Research, Karlsruhe Institute of Technology, Karlsruhe, Germany

ARTICLE INFO

Keywords:
Portugal
Weather extremes
Extreme precipitation
Dynamical systems theory
Chaos
Climate extremes

ABSTRACT

Heavy Precipitation Events (HPE) pose increasing risks to infrastructure, public safety, and water management. This study examines the dynamics and the intrinsic predictability of HPE in Portugal, focusing on the role of Atmospheric Rivers (AR). Using reanalysis data, objective weather pattern classification, and dynamical systems metrics, we show that the average AR-linked HPE exhibit 36% higher precipitation intensity than non-AR events. Primarily attributed to stronger low-level winds that increase moisture fluxes into the region, rather than a greater total column water vapor content. We employ a dynamical systems framework to evaluate the intrinsic predictability of HPE, analyzing the evolution of upper- and lower-level atmospheric fields. This allows a systematic classification of events based on their synoptic and dynamic signatures. Our findings reveal that high-predictability events are typically associated with well-defined, deep extra-tropical cyclones near [50°N, 15°W], whose mean sea-level pressure anomaly is roughly twice that of low-predictability systems. These events also exhibit enhanced jet stream interaction and more coherent Rossby wave patterns, with average precipitation intensities approximately 80% greater than those of low-predictability events. A detailed case study of the extreme mid-December 2022 event, which caused widespread flooding and damage in Western Portugal, exemplifies the interplay between AR, synoptic dynamics, and forecast confidence. Our results emphasize the value of integrating AR diagnostics with a dynamical systems perspective to improve understanding and prediction of HPE, providing a process-based foundation for enhanced forecasts in Portugal and similar mid-latitude coastal regions.

1. Introduction

The intrinsic predictability of Heavy Precipitation Events (HPE) remains a critical research priority, particularly in regions like Portugal, where such events frequently trigger severe flooding, landslides, and widespread socioeconomic disruption (Michaelides et al., 2018; Pereira et al., 2018). These high-impact events are often influenced by complex atmospheric processes, including synoptic-scale dynamics and moisture transport mechanisms such as Atmospheric Rivers (AR), which challenge traditional forecasting approaches. Improving the accuracy and lead time of HPE forecasts is key for the effectiveness of early warning systems, civil protection responses, and long-term risk reduction strategies (Merz et al., 2020). As climate change is expected to alter the frequency and intensity of HPE, advancing our understanding of the mechanisms driving HPE predictability is timely and critical for climate adaptation and disaster mitigation (Santos et al., 2019; Seneviratne et al., 2021; Araújo et al., 2022).

Atmospheric Rivers, long, narrow corridors of concentrated water vapor in the lower troposphere, play an essential role in driving HPE in Portugal (Ramos et al., 2018; Pereira et al., 2018). These transient features are capable of transporting vast amounts of moisture from tropical and subtropical regions toward mid-latitudes, where orographic lifting and frontal dynamics often convert this moisture into intense precipitation upon landfall (Gimeno et al., 2014). In the Iberian Peninsula, AR are frequently linked to wintertime HPE, especially along the western coast, where their interaction with local topography and cyclonic systems can amplify precipitation extremes (Eiras-Barca et al., 2018, 2016; Ramos et al., 2021). A striking example is the mid-December 2022 event, in which an AR made landfall in western Portugal, triggering record-breaking 24-hour accumulated precipitation totals. The resulting flooding caused widespread infrastructure damage, major transport disruptions, and significant societal and economic losses (see Section 3.3 for an in-depth analysis; Ferreira et al., 2024). Such events

* Corresponding author.
E-mail addresses: ehud.bartfeld@mail.huji.ac.il (E. Bartfeld), alexandre.ramos@kit.edu (A.M. Ramos), assaf.hochman@mail.huji.ac.il (A. Hochman).
[1] Researcher

https://doi.org/10.1016/j.wace.2026.100895
Received 21 August 2025; Received in revised form 27 February 2026; Accepted 25 March 2026
Available online 7 April 2026

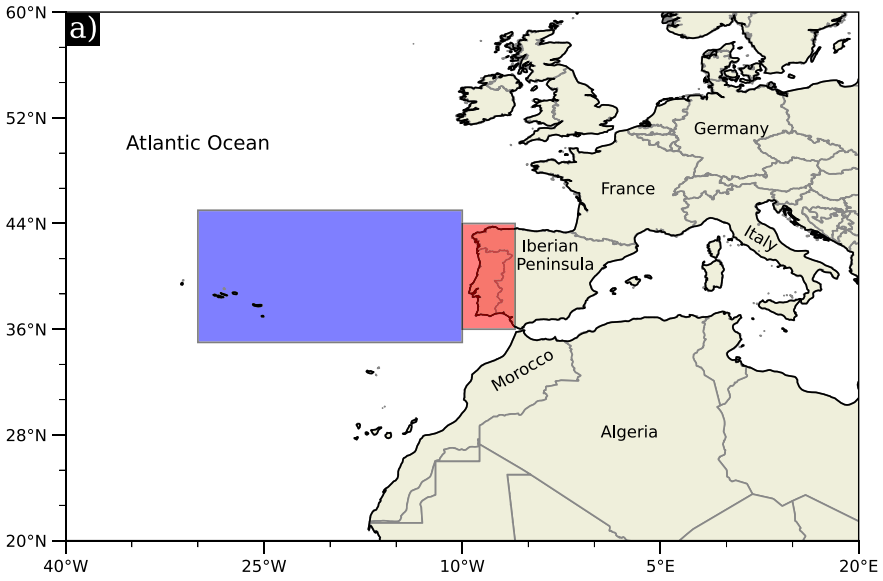

Fig. 1. The study region. The red box (34°–44°N; 6°–10°W) indicates the total precipitation and Integrated Water Vapor Transport (IVT) analyzed domain. The blue box (35°–45°N; 10°–30°W) is the domain on which the dynamical systems metrics were computed.

underscore the importance of understanding AR dynamics and their connection to regional hydro-meteorological extremes (Ramos et al., 2020).

Identifying AR typically involves analyzing Integrated Water Vapor Transport (IVT), a key diagnostic variable that quantifies the horizontal flux of water vapor within the atmosphere (Lavers et al., 2016). Measured in [$\mathrm{kg\,m^{-1}\,s^{-1}}$], IVT represents the total amount of moisture being transported through a vertical atmospheric column by winds. AR are generally detected using a combination of intensity-based thresholds and geometric criteria, such as the length, width, and coherence of the moisture plume (Lavers et al., 2012; Ramos et al., 2015). Common approaches include percentile-based thresholds, where AR are defined by IVT values exceeding the 85th or 90th percentile of the local climatological distribution (Ramos et al., 2016b), and absolute thresholds, such as IVT values greater than 250 $\mathrm{kg\,m^{-1}\,s^{-1}}$ (Ralph et al., 2019), often used in operational settings. In addition to IVT magnitude, AR detection algorithms often incorporate criteria related to the minimum length (e.g., >2000 km) and maximum width (e.g., <1000 km) to distinguish AR from broader or less-organized moisture structures.

Advanced numerical weather prediction models, reanalysis datasets, and Lagrangian diagnostics are routinely employed to visualize, track, and quantify these moisture-transport features across time and space (Ma et al., 2023). Furthermore, the orientation, duration, and landfall characteristics of IVT plumes are increasingly used to differentiate AR from other synoptic systems such as tropical plumes or frontal rain bands (Zhou et al., 2018). These refined methodologies enhance the accuracy of AR detection, enabling a more comprehensive assessment of their potential to trigger extreme precipitation, flooding, and other societal impacts, particularly in vulnerable mid-latitude coastal regions (Griffith et al., 2020). There are various methods, mostly based on IVT, to objectively track AR that were developed for different purposes, e.g., global or regional studies focusing on impacts (Rutz et al., 2019). However, while AR detection has improved considerably, understanding how these features influence the predictability of the extreme precipitation events they often trigger remains a key challenge, especially in regions like Portugal (Ramos et al., 2016a; Lavers et al., 2020).

The distinction between practical and intrinsic predictability of HPE lies in the sources and nature of the uncertainties involved. Practical predictability refers to the limitations in forecasting atmospheric states due to imperfections in numerical weather models, observational errors, and computational constraints (Slingo and Palmer, 2011). These factors limit our ability to make accurate predictions over extended time horizons. In contrast, intrinsic predictability is rooted in the inherently chaotic nature of the atmosphere, which is dictated by its sensitivity to initial conditions, as described by the butterfly effect (Lorenz, 1963). This concept implies that even with a perfect model and initial conditions, there is a fundamental limit to how far into the future accurate predictions can be made.

Dynamical systems theory is a valuable tool for quantifying the intrinsic predictability of atmospheric states, utilizing recent concepts such as local dimension (d), which estimates the number of options the atmospheric state can change to and from, and inverse persistence (θ), which estimates the time that the system stays in a region of similar states in phase space (Faranda et al., 2017). When comparing two atmospheric states, the one with higher persistence (low θ) and lower dimensionality (low d) is expected to be more predictable. (see Section 2.4 for details on the computation of these metrics; Messori et al., 2017). Recently, several studies have applied the dynamical systems framework to investigate atmospheric extremes (Hochman et al., 2019, 2021a,b, 2022, 2023a; De Luca et al., 2024, 2020; Faranda et al., 2019).

The primary objective of this study is to investigate how AR influences the dynamics and intrinsic predictability of HPE in Portugal, and to demonstrate that a single intrinsic variable can be used to map the predictability of such events. The broader goal is to apply this variable globally to other regions affected by similar AR-driven HPE. Furthermore, the region used for the dynamical systems metrics in this work serves as a synoptic common denominator for the occurrence of HPE farther inland across the European continent (e.g., Grazzini et al., 2021).

The manuscript is structured as follows: Section 2 covers the data acquisition (Section 2.1), the categorization of HPE (Section 2.2), ranking and categorizing IVT "flavors" for extreme precipitation events (Section 2.3), and the calculation of the dynamical systems metrics (Section 2.4). Section 3 discusses the synoptic and intrinsic predictability characteristics of HPE in Portugal (Section 3.1), a comparative analysis of high versus low predictability HPE associated with AR (Section 3.2), and a detailed analysis of the mid-December 2022 HPE associated with an AR (Section 3.3). Finally, Section 4 summarizes the findings and presents concluding remarks.

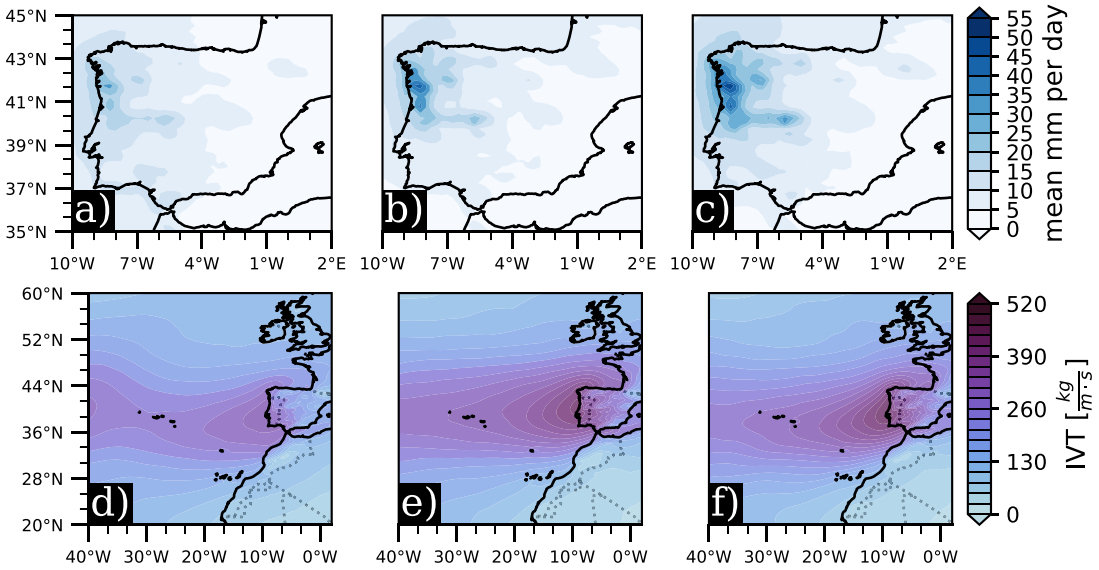

Fig. 2. The mean total daily precipitation and IVT of the different precipitation groups defined in Section 2.2. (a, d) Heavy, (b, e) IVT, and (c, f) Extreme. The precipitation data is taken over the Iberian Peninsula, while the IVT is from a more synoptic view over the northeastern Atlantic Ocean, which includes the Blue box and Red box in Fig. 1.

2. Data and methods

2.1. Data

The analysis is based on data from the ERA5 reanalysis, produced by the European Center for Medium-Range Weather Forecasts (ECMWF; Hersbach et al., 2020). ERA5 offers a comprehensive, high-resolution depiction of the atmosphere, with a spatial resolution of 0.25° × 0.25° and an hourly temporal resolution, making it well-suited for studying sub-daily atmospheric processes and extreme events. We focus on the extended winter season, i.e., October–March, for the period 1959–2023, which encompasses the climatologically most active months of HPE in Portugal (Hersbach et al., 2018b,a; Pereira et al., 2018).

To classify precipitation events and compute the dynamical systems metrics, two spatial domains were defined (Fig. 1). The Red box (34°–44°N, 6°–10°W) encompasses mainland Portugal and serves as the primary region for aggregating total daily precipitation and Integrated Water Vapor Transport (IVT). This domain was used to identify and group HPE according to intensity and AR influence. The Blue box (35°–45°N, 10°–30°W) is located over the eastern North Atlantic Ocean, west of Portugal, a key region for the formation and evolution of synoptic-scale systems that influence extreme winter precipitation over the Iberian Peninsula (Ramos et al., 2014a). Two additional regions were used to validate the choice of the Blue box (Figure S1). The results show that the relationships among all precipitation groups are similar (Figure S2). This is consistent with previous studies (Hochman et al., 2022), which demonstrated that, as long as the key synoptic features are contained within the selected region, the resulting behavior remains unchanged. For consistency with previous work, the Blue box was selected for the analysis.

To assess the dynamical characteristics and intrinsic predictability of HPE, we calculated daily-mean horizontal wind magnitudes within the Blue box at standard pressure levels from 1000 to 300 hPa, in 100 hPa increments. These wind fields served as the basis for computing the dynamical systems metrics (see Section 2.4). The goal was to connect the large-scale flow patterns over the Atlantic to the intrinsic predictability of classified HPE in the Red box, thereby linking remote flow dynamics with local hydro-climatic impacts.

2.2. Categorizing precipitation groups

To assess the role of Atmospheric Rivers (AR) in the intrinsic predictability of heavy precipitation events (HPE), we classify the full set of 11,664 events into three precipitation-based subgroups:

1. **IVT Events:** These events are defined using daily mean integrated water vapor transport (IVT), computed as:

$$IVT = \frac{1}{g}\left\|\int q\vec{V}\,dp\right\| \tag{1}$$

where q is the specific humidity, V is the horizontal wind vector, dp is the pressure difference between adjacent vertical levels, and g is the gravitational acceleration. A threshold IVT value was determined for each grid point within the analysis region (Fig. 1; red box) using the 85th percentile of the mean daily IVT (Ramos et al., 2015). An event was classified as an IVT event if ≥85% of the grid points exceeded their local threshold — in total 594 events.
2. **Heavy Events:** This group includes only events with a domain-averaged daily precipitation of at least 1 mm, thereby excluding dry days. Within this subset, we applied a percentile-based classification using the 98th-percentile daily precipitation at each grid point. An event was considered a Heavy Event if >2% of the grid points exceeded their local thresholds. The 2% threshold was chosen to yield approximately 10% of all wet events, about 17 per year, classified as Heavy, thereby focusing on spatially localized but intense precipitation — in total 1085 events.
3. **Extreme Events:** These are defined as the intersection of the IVT and Heavy Precipitation groups. Events in this category simultaneously meet the IVT and heavy precipitation criteria described above — in total 298 events.

2.3. Characterizing integrated water vapor transport flavors

This study investigates heavy precipitation events influenced by AR, identified using IVT, a composite metric that combines specific humidity and wind magnitude (see Section 2.2; Ramos et al., 2016a). To explore which of these variables exhibits a stronger deterministic relationship with extreme precipitation, we adopt the AR "flavor"

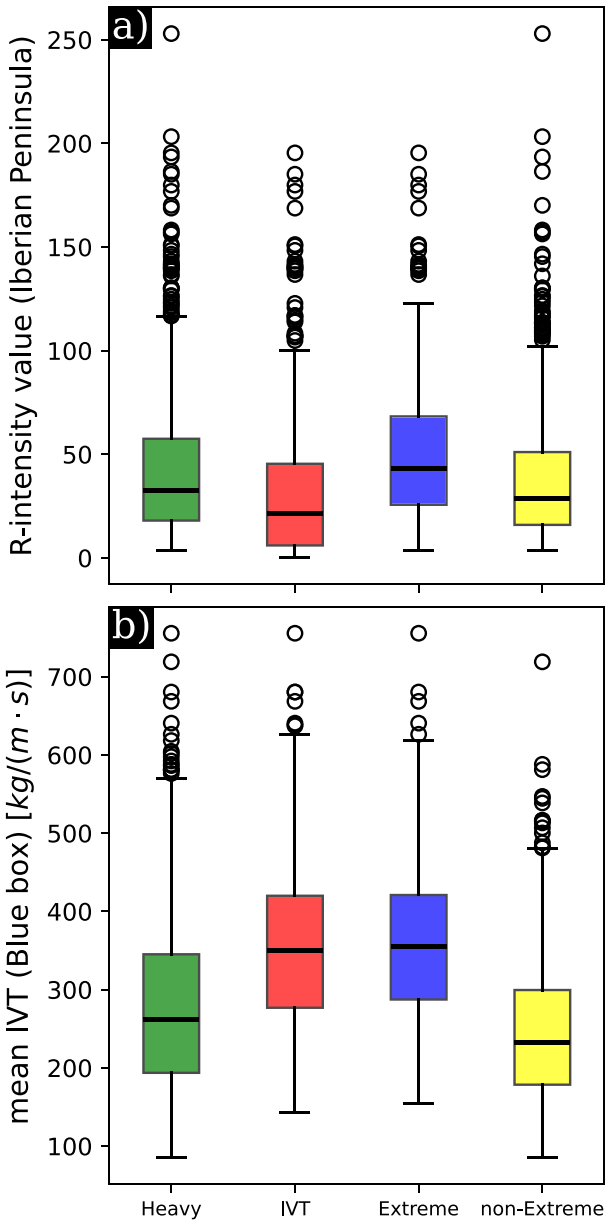

Fig. 3. Box plots of the precipitation sub-groups (Section 2.2) including non-Extreme (events classified as Heavy but not Extreme). (a) mean daily precipitation R-intensity values (Section 2.3) over the Iberian Peninsula (35°–45°N, 10°W–2°E), mean values of 42, 32, 53, 39, and standard deviation of 34, 34, 36, 32 for Heavy, IVT, Extreme, and non-Extreme, respectively. (b) mean daily IVT value in the Blue box (Section 2.1) mean values of 278, 357, 363, 246, and standard deviation of 108, 104, 107, and 90 for Heavy, IVT, Extreme, and non-Extreme, respectively.

framework (Gonzales et al., 2020). This method characterizes AR along a continuum from "wet" (moisture-dominated IVT) to "windy" (wind-dominated IVT), enabling a more nuanced assessment of whether moisture or wind plays the leading role in driving AR-related precipitation extremes described as:

$$IVTq' = \frac{1}{g}\sqrt{\left(\int q\bar{u}dp\right)^2 + \left(\int q\bar{v}dp\right)^2}$$
$$IVTu'v' = \frac{1}{g}\sqrt{\left(\int \bar{q}udp\right)^2 + \left(\int \bar{q}vdp\right)^2} \quad (2)$$

where $IVTq'$ represents the moisture-dominated component of IVT, calculated by applying a 30-day moving average to the wind velocity components ($\bar{u}$, $\bar{v}$; Gonzales et al., 2020) but using a shorter averaging window due to the limited seasonal focus of this study. Conversely, $IVTu'v'$ represents the wind-dominated component, obtained by applying the moving average to the specific humidity ($\bar{q}$). To integrate IVT "flavors" across vertical levels, we used the ERA5 reanalysis dataset, which provides data from 1000 hPa to 300 hPa (Hersbach et al., 2018a). The integration was performed over the designated Blue box region (Fig. 1), allowing us to connect the large-scale AR characteristics over the ocean with the categorized precipitation groups over land. To complement the moisture–wind dominance analysis, we employed a ranking method for precipitation events based on both intensity and spatial extent (Ramos et al., 2014b). Specifically, we applied this ranking to all events with a domain-averaged daily precipitation greater than 1 mm. For each grid point in the daily mean field, a measure of normalized event rarity was computed as:

$$R_{i,j} = \frac{P_{i,j} - \mu_{i,j}}{\sigma_{i,j}} \quad (3)$$

Here, $R_{i,j}$ denotes the event rarity at grid point (i, j) defined as the standardized anomaly of precipitation for a given event. Where $P_{i,j}$ is the precipitation at grid point (i, j). $\mu_{i,j}$ is the climatological mean, and $\sigma_{i,j}$ is the standard deviation of precipitation across all events at that location. Following this, the standard deviation of $R_{i,j}$ denoted $\sigma_{R_{i,j}}$ was calculated to normalize the rarity threshold.

To quantify the overall extremeness of each daily event, we computed an R-intensity value:

$$R = A \times M \quad (4)$$

where M is the mean rarity of all grid points exceeding a threshold of $2\sigma_{R_{i,j}}$, and A is the fraction of grid points within the domain that surpass this threshold on that day. This method provides a single scalar R-intensity value for each event by integrating the severity and spatial extent of extreme precipitation, thereby facilitating comparisons across events.

2.4. Computing dynamical systems metrics

The atmosphere can be described as a chaotic dynamical system (Lorenz, 1963). To characterize its local dynamical behavior, a framework combining extreme value theory (EVT) and Poincaré recurrences has been introduced (Lucarini et al., 2016; Faranda et al., 2017). This approach enables the estimation of dynamical indicators from discrete-time datasets such as atmospheric reanalyses. For instance, each daily 2-D wind field at selected pressure levels (from 1000 to 300 hPa in 100 hPa intervals) over a target region (e.g., the Blue box in Fig. 1) can be interpreted as a single point along the system's trajectory in phase space. The analysis focuses on computing two metrics for each atmospheric state, i.e., each wind map: the local dimension (d) and the persistence (θ^{-1}). These are evaluated at a reference state ξ, representing a particular time in the dataset. Letting $x(t)$ represent the system's trajectory and using the Euclidean distance, we define the logarithmic return:

$$g(t) = -\log(\mathrm{dist}(x(t), \xi)) \quad (5)$$

Here, $g(t)$ is high when the system's state closely resembles ξ and low when far from ξ. To identify significant recurrences, we select time steps where $g(t)$ exceeds a high threshold $s(q, \xi)$, defined by a high quantile q, in our case, the 98th percentile of the series g. The exceedances are then:

$$u(t) = g(t) - s(q, \xi) \quad (6)$$

The cumulative distribution of these exceedances, $F(u, \xi)$, converges under appropriate conditions to the exponential form of the Generalized Pareto Distribution (GPD):

$$F(u, \xi) \simeq e^{\left(-\vartheta(\xi)\frac{u(\xi)}{\sigma(\xi)}\right)} \quad (7)$$

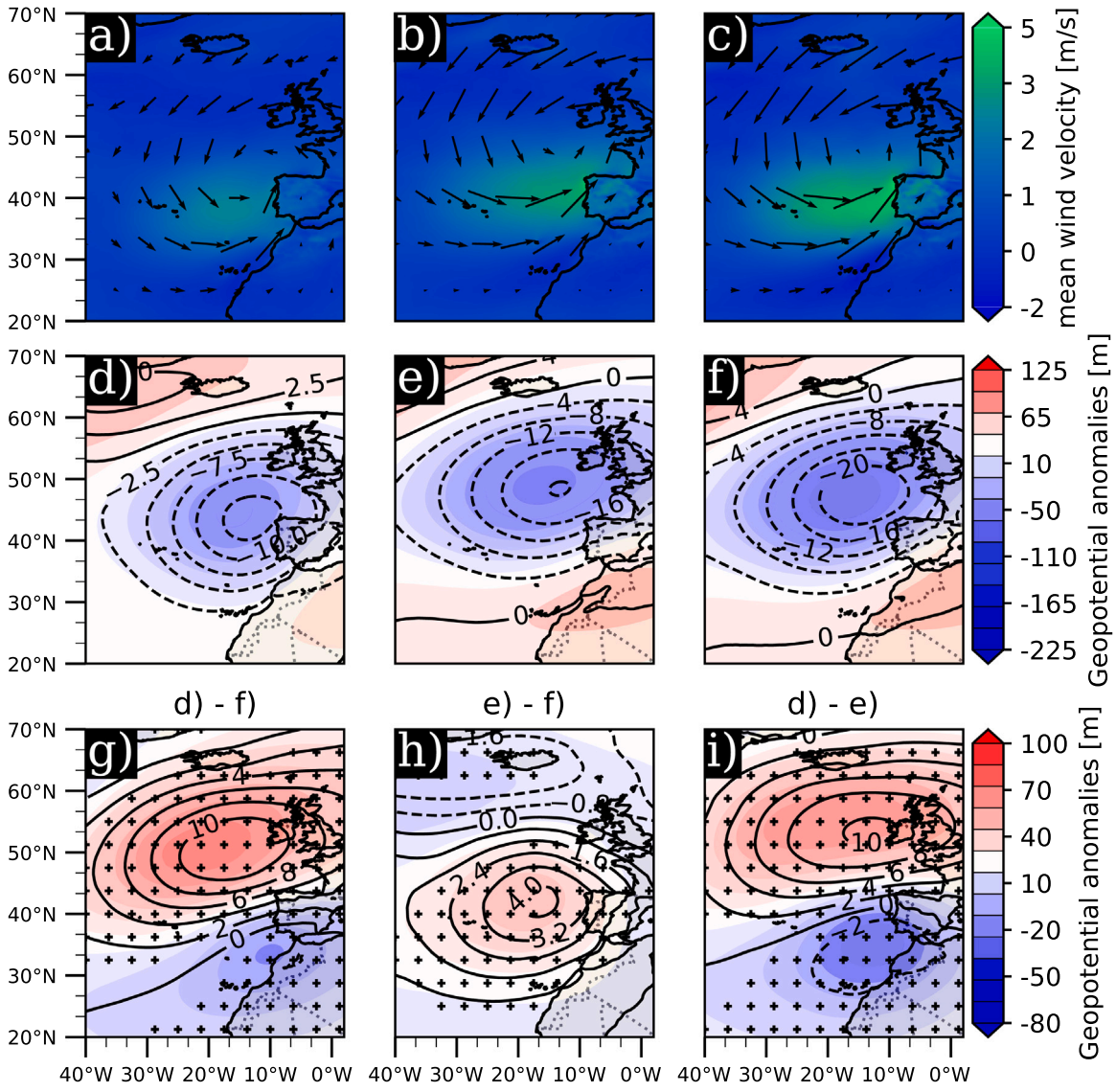

Fig. 4. Synoptic analysis of the Heavy (a, d), IVT (b, e), and Extreme (c, f) precipitation groups (see Section 2.2). Top row (a–c): Mean 10-meter wind anomalies (direction and speed; m s^{-1}). Middle row (d–f): Mean anomalies of 500 hPa geopotential height (color shading; m) and sea level pressure (black contours; hPa). Bottom row (g–i): Pairwise differences in anomalies between groups: (g) Heavy–Extreme, (h) IVT–Extreme, (i) Heavy–IVT. Black crosses denote grid points with statistically significant differences at the 5% level using a two-sided T-test.

Here, ϑ is the extremal index calculated using the Süveges maximum likelihood estimator (Süveges, 2007), and $\sigma(\xi)$ is a scale parameter depending on the state ξ. The local dimension is then given by:

$$d(\xi) = \frac{1}{\sigma(\xi)} \tag{8}$$

And the persistence is calculated as:

$$\theta^{-1}(\xi) = \frac{\Delta t}{\vartheta(\xi)} \tag{9}$$

where Δt is the time step between observations, in our case, one day. The Local dimension (d) reflects how complex the system's behavior is around the state ξ; a higher d indicates more degrees of freedom and lower predictability. The persistence θ^{-1} quantifies how long the system remains near ξ; high persistence implies long-lasting states, while $\theta^{-1} = 1$ indicates transient behavior. Further details can be found in the literature (e.g., Lucarini et al., 2016; Faranda et al., 2019; Hochman et al., 2023a). The metrics in this work were calculated using a MATLAB package (see Data Availability Statement).

3. Results

3.1. Synoptic and dynamical systems characterization of precipitation extremes in Portugal

After classifying the precipitation sub-groups as defined in Section 2.2, composite mean total precipitation and the corresponding synoptic mean daily IVT were plotted to establish a qualitative distinction between the groups (Fig. 2). These groups were designed to distinguish between HPE with and without high IVT, allowing us to assess the role of AR in the intrinsic predictability of HPE. The Extreme Precipitation sub-group exhibits the highest mean total precipitation (Fig. 2c with a, b). It also shows the highest mean R-intensity value

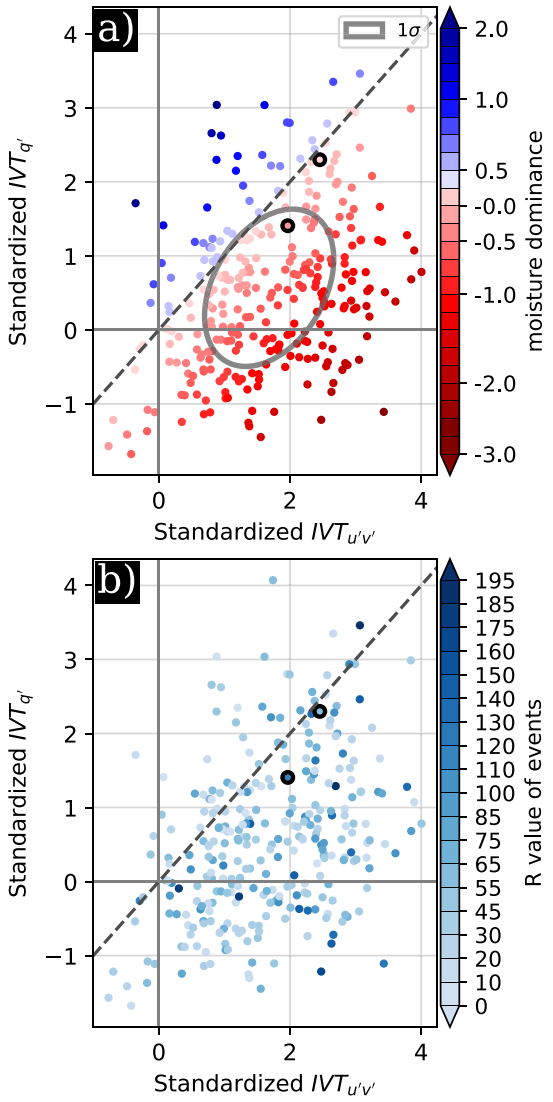

Fig. 5. The Extreme Precipitation group (see Section 2.2) is shown in moisture–wind space, defined by $IVTq'$ and $IVTu'v'$ (see Section 2.3). (a) Events are colored by moisture dominance, quantified as the distance from the neutral line $y = x$: blue indicates more moisture-dominated events, red indicates more wind-dominated ones. A 1-standard-deviation covariance ellipse is shown. (b) Events are colored by their R-ranked value (see Section 2.3 following the methodology of Ramos et al., 2014b), which accounts for both precipitation intensity and spatial extent. The two black-encircled points correspond to the December 2022 event, including 12 and 13 December.

(53; see Fig. 3a), compared to 42 for the Heavy Precipitation group and 39 for the non-AR-related Heavy Precipitation group, with comparable standard deviations across groups, i.e., 36, 34, and 32, respectively.

The synoptic IVT patterns (Fig. 2d–f) reveal that both the IVT and Extreme groups exhibit stronger and more elongated IVT structures than the Heavy group (cf. Fig. 2e, f with d). This behavior reflects characteristic features of AR, which are known drivers of HPE in Portugal (Section 1). Box plots in Fig. 3b show the daily mean IVT value in the Blue box region (Section 2.1), where the main characteristics of AR are most prominent. Notably, the Extreme group again has a higher mean IVT (363) than the Heavy and non-AR-related groups (278 and 246, respectively), and the standard deviations are similar (108, 107, and 90). These findings further support our approach of extrapolating from data in the Red box to dynamical systems analysis in the Blue box, as detailed below.

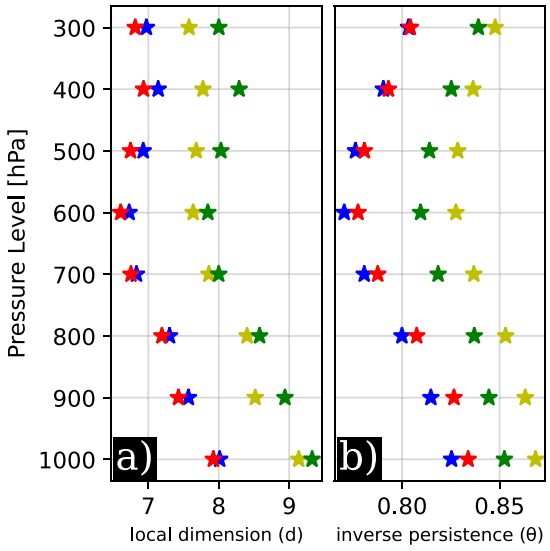

Fig. 6. Comparison of local dimension (d) and inverse persistence (θ) for the Extreme (blue), IVT (red), Heavy (green), and Heavy without Extreme (yellow) precipitation groups (see Section 2.2). Both metrics were computed at multiple pressure levels using the average magnitude of the vector wind field. This analysis characterizes the intrinsic predictability of each group as a function of atmospheric depth.

To confirm that the Extreme group indeed represents true extreme precipitation events, we performed a synoptic evaluation of total precipitation, near-surface wind speeds, 500 hPa geopotential height, and mean sea level pressure (Fig. 4). The analysis reveals that the Extreme group (Fig. 4c) is characterized by stronger low-level wind anomalies compared to the other groups, highlighting the role of anomalous moisture transport typically associated with atmospheric rivers. Additionally, this group exhibits a pronounced low-pressure anomaly centered northwest of the region of interest, both at the surface and aloft. These features, i.e., enhanced wind anomalies and a deep, displaced low-pressure system, are consistent with known signatures of extreme precipitation events in the region, further validating the group classification (Ferreira et al., 2024).

Building on this synoptic characterization, we next examine the relative contributions of wind and moisture to IVT intensity during these events. To assess which variable, moisture or wind, plays a greater role in driving extreme precipitation events, we applied the IVT "flavors" methodology, which decomposes IVT into its moisture and wind components (see Section 2.3). Each component was normalized, and the Extreme Precipitation group was then analyzed in moisture–wind space (Fig. 5), where each of the 298 events is plotted relative to the neutral 1:1 line. Notably, 251 of these events fall below this line, indicating that most extreme events are more strongly influenced by wind anomalies than by specific humidity anomalies.

To further characterize the distribution, we plotted a 1-standard-deviation covariance confidence ellipse for the Extreme group (Fig. 5a). The ellipse is centered at (1.68, 0.56) in the normalized space. I.e., 1.68 standard deviations in the wind direction (X-axis) and 0.56 in the moisture direction (Y-axis) from the general event population mean (0, 0). This offset confirms that extreme events in our dataset are driven more by unusually strong wind contributions to IVT rather than by exceptional moisture levels, underscoring the dynamical nature of these high-impact events. R-intensity values were computed relative to the full event database (Fig. 5b) to assess the severity of precipitation across different IVT "flavor" sub-groups. The distributions of R-intensity values for both the wind-dominated and moisture-dominated extreme events closely resemble that of the whole Extreme group, suggesting that both types can produce intense precipitation. However, when

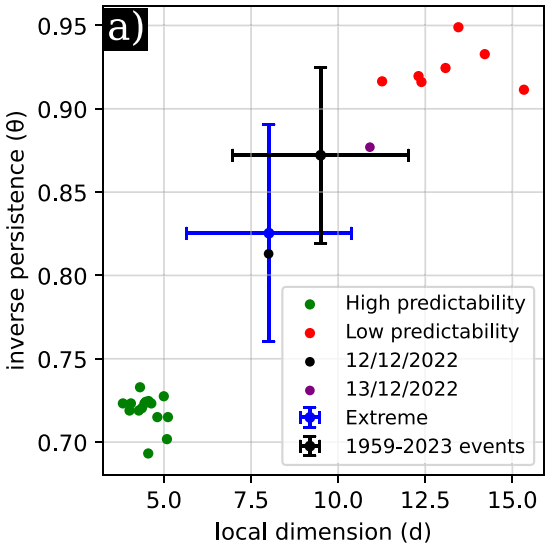

Fig. 7. Scatter plot of local dimension (d) versus inverse persistence (θ), calculated using the average wind vector at 1000 hPa. Mean positions with standard deviation bars for the Extreme group (see Section 2.2) and the entire database used in this work are added. Green points represent high-predictability events (lowest decile of both d and θ in the Extreme group), while red points indicate low-predictability events (highest decile of both metrics). The blue and purple points correspond to the mid-December 2022 case study events, labeled accordingly.

comparing only the upper 20th percentile of events, wind-dominated extremes show a substantially greater mean deviation from the neutral 1:1 line in IVT space, i.e., 1.1 standard deviations, compared to just 0.26 for moisture-dominated events. This suggests that while high R-intensity events occur in both subtypes, the dynamical contribution from wind anomalies tends to be more pronounced than that from specific humidity, thereby reinforcing the notion that wind plays a central role in generating the most intense events.

Building on this, the IVT "flavors" analysis suggests that wind anomalies are the dominant factor shaping extreme precipitation events. To further explore the dynamical nature of these events, we analyzed the local dimension (d) and inverse persistence (θ), two indicators of intrinsic atmospheric predictability, using the magnitude of the wind field as the input variable. These metrics were computed at various pressure levels for each precipitation group (Fig. 6). Across all groups, d and θ exhibit a clear vertical structure, with all decreasing with height from 1000 hPa to 300 hPa, indicating an increase in persistence and lower dimensionality at upper levels. Notably, the Extreme and IVT groups show consistently lower mean values of d and θ across levels, whereas the Heavy and non-extreme groups do not. This pattern suggests that extreme events, particularly those associated with strong IVT, occur in more constrained dynamical states and are thus potentially more predictable in a flow-dependent framework. The similarity in d and θ between the Extreme and IVT groups further supports the view that strong wind-driven IVT is a defining dynamical feature of high-impact precipitation events.

3.2. Quantifying the synoptic influence on the intrinsic predictability of heavy precipitation events associated with atmospheric rivers

Local dimension (d) and inverse persistence (θ) were calculated using wind magnitude at 1000 hPa (Fig. 7), serving as indicators of the intrinsic predictability of the atmospheric state. From the Extreme precipitation group, we selected 15 high-predictability events and seven low-predictability events based on the lowest and highest deciles, respectively, of both d and θ. To further explore the dynamical differences between these two subsets, we analyzed their associated synoptic anomalies and precipitation patterns (Fig. 8).

High-predictability events (Fig. 8a, d, g) were associated with more coherent and pronounced synoptic features, including strong and well-organized southwesterly low-level winds (Fig. 8a) and a deeper low-pressure anomaly centered near 50°N, 15°E (Fig. 8d). The central sea level pressure anomaly in these events averaged −40.6 hPa, nearly double that of the low-predictability group (−20.6 hPa; Fig. 8e), indicating a more dynamically active environment. These events also produced more widespread and intense precipitation, with higher average daily totals across a broader area (Fig. 8g–i).

In contrast, low-predictability events were associated with weaker and less spatially organized circulation patterns and confined precipitation footprints (Fig. 8b, e, h). Their lower R-intensity values and more localized impacts reflect a reduced dynamical signal. Quantitatively, high-predictability events exhibited significantly higher mean R-intensity values (70 vs. 39) and greater variability (standard deviations of 40 vs. 31), suggesting that greater atmospheric organization supports both enhanced precipitation and predictability (Hochman et al., 2022).

The next section applies the framework to the December 2022 case study, a well-documented high-impact event. This example illustrates how the dynamical-systems metrics evolve in time and relate to the underlying synoptic development, demonstrating their added value beyond a purely climatological perspective.

3.3. The December 2022 case study

The December 2022 event was characterized by record-breaking rainfall over the 24 h period from 12 to 13 December. A total of 120.3 mm was recorded at the historic Dom Luiz Observatory in Lisbon, Portugal, the highest 24-hour total in over 160 years of observations (Ferreira et al., 2024). Despite analyzing each day independently, our classification method identified both 12 and 13 December as Extreme precipitation events, reinforcing its sensitivity to high-impact occurrences even without aggregating over longer durations.

The event's R-intensity values were exceptionally high, 56.4 on 12 December and 115.6 on 13 December, ranking it among the most intense in the dataset. When evaluated over the 24-hour maximum rainfall period (e.g., 12 December 15 UTC to 13 December 15 UTC), total precipitation reached 134.6 mm (Ferreira et al., 2024; Dias, 2022; IPMA, 2023), suggesting the potential for even higher R values under sub-daily evaluation. This highlights the importance of temporal resolution in early warning systems and disaster preparedness frameworks.

From an IVT "flavor" perspective, the event exhibited a slight wind dominance, with normalized values reaching 2.5 and 2.0 standard deviations for the windy component and 2.3 and 1.4 for the wet component on the 12th and 13th, respectively (Fig. 5). This combined anomaly highlights a key dynamical feature of AR events: strong low-level winds acting as an efficient moisture conveyor belt. The December case illustrates how both dynamic and thermodynamic contributions are required to generate extreme precipitation, but with wind-driven moisture transport (i.e., AR dynamics) playing a leading role.

Forecasting implications emerge clearly when considering the event's evolution in the dynamical systems space (Fig. 7). On 12 December, the system displayed relatively low values of local dimension (d) and inverse persistence (θ), placing it within one standard deviation of the Extreme precipitation group mean, indicative of a more predictable atmospheric state. By 13 December, as the event intensified, both d and θ exceeded the 1-standard-deviation threshold, indicating reduced predictability. This transition suggests that while the onset of such AR-driven events may be forecastable with greater confidence, their intensification, especially as synoptic structures deepen, can reduce forecast skill due to increased system complexity and sensitivity to initial conditions.

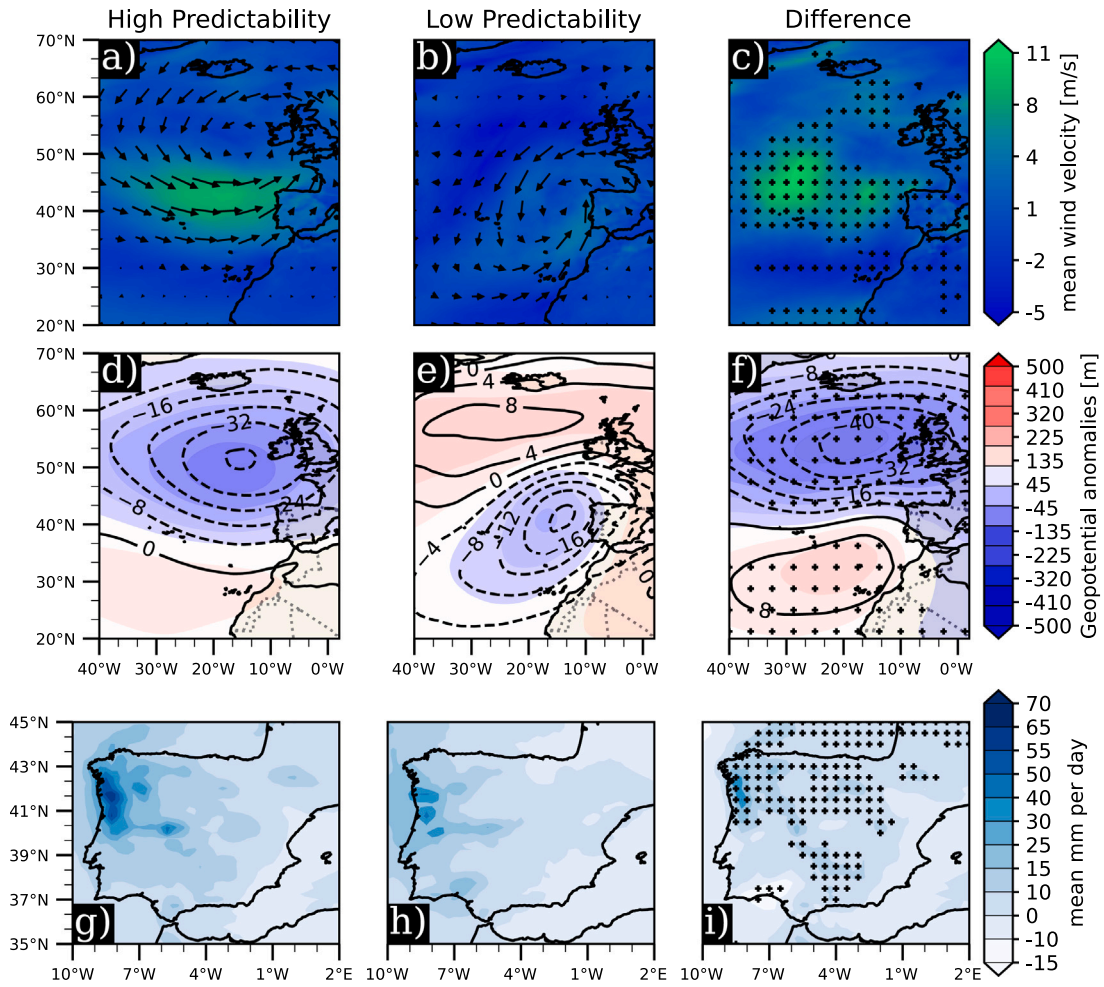

Fig. 8. Synoptic analysis of high- (a, d, g) and low-predictability (b, e, h) events within the Extreme precipitation group (see Fig. 7). Panels c, f, and i show the differences between high- and low-predictability composites, with black crosses indicating grid points where the difference is statistically significant using a two-sided T-test at the 5% level. Top row: Mean anomalies of 10-meter wind vectors (direction and speed; m s^{-1}). Middle row: Mean anomalies of 500 hPa geopotential height (color shading; m) and sea level pressure (black contours; hPa). Bottom row: Mean total precipitation (mm).

The accompanying synoptic analysis (Fig. 9) supports this interpretation. On 12 December, a classic AR-like structure is observed, with elongated, coherent wind anomalies extending from the tropics toward Iberia, consistent with strong poleward moisture transport. By 13 December, the circulation had evolved into a deep, well-defined low-pressure anomaly centered over Portugal, enhancing dynamical uplift and precipitation efficiency. This evolution from an AR-like conveyor to a fully developed mid-latitude cyclone illustrates the hybrid nature of many extreme winter events. It underlines the challenge for forecasters in capturing both the initiation and rapid intensification stages.

In summary, the December 2022 case highlights the dual importance of AR dynamics and intrinsic atmospheric predictability in shaping extreme precipitation events. It underscores the forecast value of identifying early AR signatures and the need for high-resolution tools to anticipate transitions into more chaotic, low-predictability states as cyclones mature.

4. Discussion and conclusions

This study provides new insights into the dynamics and predictability of heavy precipitation events (HPE) in Portugal's winter season, with particular emphasis on the role of atmospheric rivers (AR). Our results confirm previous findings that AR-linked events tend to produce substantially higher precipitation totals than non-AR events (Ramos et al., 2015; Eiras-Barca et al., 2016), underscoring their critical influence in shaping extreme rainfall over the Iberian Peninsula. Importantly, we find that the wind magnitude, rather than atmospheric moisture content alone, is the primary driver of IVT during these events, consistent with the conceptual framework proposed by Gonzales et al. (2020). This distinction highlights the forecasting value of low-level wind fields in the detection and characterization of AR. Using a combination of synoptic evaluation, IVT "flavor" diagnostics, and dynamical systems metrics, we classified precipitation events by their underlying structure and intrinsic predictability. Specifically, high predictability HPE are associated with large amplitude atmospheric waves, characterized by strong zonal southwesterly flow and pronounced low-pressure anomalies northwest of the region. These events exhibited low values of local dimension and inverse persistence, indicating that the atmospheric state was more constrained and thus more predictable (Hochman et al., 2019, 2021b, 2022). This is consistent with recent efforts to quantify forecast confidence through dynamical systems approaches (Vakrat and Hochman, 2023).

In contrast, low-predictability HPE were linked to more complex and less stable meteorological settings, including rapidly developing extra-tropical cyclones and enhanced meridional flow. These systems often undergo explosive development before reaching the Iberian Peninsula, with dynamics strongly influenced by diabatic processes such as latent heat release and low-level warm air advection (Ribeiro et al., 2022; Liberato et al., 2011). Such processes typically occur on spatial scales smaller than those resolved in global weather models,

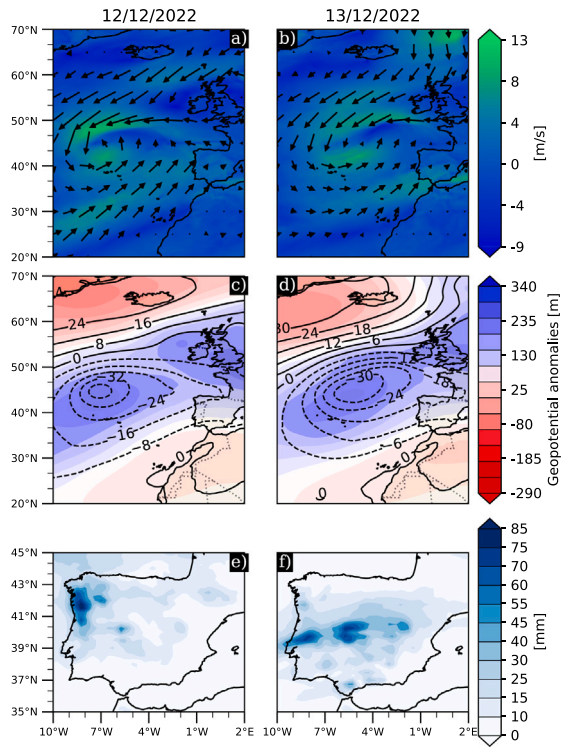

Fig. 9. Synoptic analysis of the December 2022 case study event. (a, c, e) 12 December 2022. (b, d, f) 13 December 2022. Top row: Anomalies of 10-meter wind speed and direction (m s^{-1}). Middle row: Anomalies of 500 hPa geopotential height (color shading; m) and sea level pressure (black contours; hPa). Bottom row: Total daily precipitation (mm).

complicating real-time forecasting. The observed reduction in predictability under these configurations is consistent with the theoretical limitations of capturing sub-synoptic energy conversions and wave interactions (Charney, 1947; Hoskins et al., 1985).

The December 2022 case study offers a practical demonstration of these principles. Record-breaking rainfall (134.6 mm in 24 h; Ferreira et al., 2024) was associated with an intense AR event that was flagged independently on both days of occurrence. Synoptic and dynamical analysis revealed that the system transitioned from a more to a less predictable state as precipitation intensified, underscoring the temporal variability in forecast confidence. The IVT signature of this event exhibited high wind-dominated values with secondary moisture contributions, supporting its AR classification and affirming the value of IVT "flavor" analysis in distinguishing between different types of extreme precipitation events.

The results should be interpreted with several caveats. The use of ERA5 daily means and a fixed October–March season likely smooths short-lived extremes and under represents mesoscale processes that often govern peak rainfall. The dynamical-systems metrics, derived from wind magnitude in an upstream Atlantic domain, capture large-scale flow organization but do not explicitly account for moisture variability, diabatic processes, or land–atmosphere interactions. Finally, while composites and the December 2022 case study provide physical insight, they cannot fully represent event-to-event diversity or ensure the transferability of the results beyond Portugal without further evaluation.

Taken together, our results demonstrate the utility of combining AR diagnostics with a dynamical-systems perspective to better understand and anticipate HPE. From an operational standpoint, the framework offers a flow-dependent measure of forecast confidence: low values of local dimension and inverse persistence flag dynamically constrained states in which deterministic forecasts are more likely to be reliable, whereas higher values warn of rapidly evolving, low-predictability regimes. In practice, identifying cyclone configurations that promote efficient AR landfall, characterized by coherent low-level jets, strong IVT, and well-organized upper-level support, can provide forecasters with early cues on both event severity and the expected robustness of forecasts (Hochman et al., 2023b; Hoy et al., 2014). When used alongside ensemble spread and conventional AR detection tools, these metrics can help prioritize situations requiring heightened preparedness, targeted ensemble interrogation, or rapid forecast updates. More broadly, this approach aligns with emerging efforts to identify "windows of opportunity" for sub-seasonal to seasonal prediction of extremes, by linking large-scale flow organization to predictable intervals in which high-impact precipitation events are more likely to occur and be forecast with increased confidence (Sillmann et al., 2017; Mariotti et al., 2020; Lembo et al., 2024).

Ultimately, although this study focused on Portugal, its implications are broader. The methodological framework may apply to other mid-latitude regions influenced by AR, such as the western coasts of North and South America and southern Africa (e.g., Lavers and Villarini, 2013; Huang et al., 2021; Chapman et al., 2019). Enhancing the ability to quantify the predictability of such events has clear value for impact mitigation and risk management, especially under a changing climate.

CRediT authorship contribution statement

Ehud Bartfeld: Writing – review & editing, Writing – original draft, Visualization, Software, Formal analysis, Data curation. **Alexandre M. Ramos:** Writing – review & editing, Writing – original draft, Methodology, Funding acquisition, Conceptualization. **Assaf Hochman:** Writing – review & editing, Writing – original draft, Supervision, Project administration, Methodology, Funding acquisition, Conceptualization.

Declaration of Generative AI and AI-assisted technologies in the writing process

During the preparation of this work, the authors used ChatGPT-5.2 and Grammarly to improve language and readability. After using this tool, the authors reviewed and edited the content as needed and take full responsibility for the publication's content.

Funding

The Israel Science Foundation (grant #978/23) and the Planning and Budgeting Committee of the Israeli Council for Higher Education, under the 'MedWORLD' Consortium, provide funding for EB and AH's participation. In addition, the COST Actions CA19109 'MedCyclones' and CA22162 'FutureMed', supported by COST (European Cooperation in Science and Technology), support AH's contribution. This work was carried out within the framework of the AMOTHEC project (DRI/India/0098/2020; DOI: 10.54499/DRI/India/0098/2020), funded by the Fundação para a Ciência e a Tecnologia (FCT) I.P./ MCTES, Israel. AMR was supported by the Helmholtz "Changing Earth — Sustaining our Future" program, Israel.

Declaration of competing interest

The authors declare that they have no known competing financial interests or personal relationships that could have appeared to influence the work reported in this paper.

Acknowledgment

The authors acknowledge the European Center for Medium-range Weather Forecasts (ECMWF) for providing open-source data used in this study.

Appendix A. Supplementary data

Supplementary material related to this article can be found online at https://doi.org/10.1016/j.wace.2026.100895.

Data availability

Data will be made available on request.

References

Araújo, J.R., Ramos, A.M., Soares, P.M., Melo, R., Oliveira, S.C., Trigo, R.M., 2022. Impact of extreme rainfall events on landslide activity in Portugal under climate change scenarios. Landslides 19 (10), 2279–2293.

Chapman, W., Subramanian, A., Delle Monache, L., Xie, S., Ralph, F., 2019. Improving atmospheric river forecasts with machine learning. Geophys. Res. Lett. 46 (17–18), 10627–10635.

Charney, J.G., 1947. The dynamics of long waves in a baroclinic westerly current. J. Atmos. Sci. 4 (5), 136–162.

De Luca, P., Braam, M., Komacek, T.D., Hochman, A., 2024. The impact of ozone on earth-like exoplanet climate dynamics: the case of proxima centauri b. Mon. Not. R. Astron. Soc. 531 (1), 1471–1482.

De Luca, P., Messori, G., Faranda, D., Ward, P.J., Coumou, D., 2020. Compound hot-dry and cold-wet dynamical extremes over the mediterranean. Earth Syst. Dyn. Discuss. 2020, 1–24.

Dias, D., 2022. Vivemos o dia de Dezembro em que mais choveu em Lisboa. URL https://www.publico.pt/2022/12/13/azul/noticia/vivemos-dia-dezembro-choveu-lisboa-2031336.

Eiras-Barca, J., Brands, S., Miguez-Macho, G., 2016. Seasonal variations in North Atlantic atmospheric river activity and associations with anomalous precipitation over the Iberian Atlantic Margin. J. Geophys. Res.: Atmospheres 121 (2), 931–948.

Eiras-Barca, J., Ramos, A.M., Pinto, J.G., Trigo, R.M., Liberato, M.L., Miguez-Macho, G., 2018. The concurrence of atmospheric rivers and explosive cyclogenesis in the North Atlantic and North Pacific basins. Earth Syst. Dyn. 9 (1), 91–102.

Faranda, D., Messori, G., Vannitsem, S., 2019. Attractor dimension of time-averaged climate observables: insights from a low-order ocean-atmosphere model. Tellus A: Dyn. Meteorol. Ocean. 71 (1), 1554413.

Faranda, D., Messori, G., Yiou, P., 2017. Dynamical proxies of North Atlantic predictability and extremes. Sci. Rep. 7 (1), 41278.

Ferreira, T.M., Trigo, R.M., Gaspar, T.H., Pinto, J.G., Ramos, A.M., 2024. The record-breaking precipitation event of december 2022 in Portugal. Nat. Hazards Earth Syst. Sci. Discuss. 2024, 1–21.

Gimeno, L., Nieto, R., Vázquez, M., Lavers, D.A., 2014. Atmospheric rivers: A mini-review. Front. Earth Sci. 2, 2.

Gonzales, K.R., Swain, D.L., Barnes, E.A., Diffenbaugh, N.S., 2020. Moisture-versus wind-dominated flavors of atmospheric rivers. Geophys. Res. Lett. 47 (23), e2020GL090042.

Grazzini, F., Fragkoulidis, G., Teubler, F., Wirth, V., Craig, G.C., 2021. Extreme precipitation events over northern Italy. Part II: Dynamical precursors. Q. J. R. Meteorol. Soc. 147 (735), 1237–1257.

Griffith, H.V., Wade, A.J., Lavers, D.A., Watts, G., 2020. Atmospheric river orientation determines flood occurrence. Hydrol. Process. 34 (23), 4547–4555.

Hersbach, H., Bell, B., Berrisford, P., Biavati, G., Horányi, A., Muñoz Sabater, J., Nicolas, J., Peubey, C., Radu, R., Rozum, I., Schepers, D., Simmons, A., Soci, C., Dee, D., Thépaut, J.-N., 2018a. ERA5 hourly data on single levels from 1940 to present. Copernicus climate change service (C3S) climate data store (CDS). http://dx.doi.org/10.24381/cds.bd0915c6, URL https://cds.climate.copernicus.eu/datasets/reanalysis-era5-pressure-levels?tab=overview.

Hersbach, H., Bell, B., Berrisford, P., Biavati, G., Horányi, A., Muñoz Sabater, J., Nicolas, J., Peubey, C., Radu, R., Rozum, I., Schepers, D., Simmons, A., Soci, C., Dee, D., Thépaut, J.-N., 2018b. ERA5 hourly data on single levels from 1940 to present. Copernicus climate change service (C3S) climate data store (CDS). http://dx.doi.org/10.24381/cds.bd0915c6, URL https://cds.climate.copernicus.eu/datasets/reanalysis-era5-single-levels?tab=documentation.

Hersbach, H., Bell, B., Berrisford, P., Hirahara, S., Horányi, A., Muñoz-Sabater, J., Nicolas, J., Peubey, C., Radu, R., Schepers, D., et al., 2020. The ERA5 global reanalysis. Q. J. R. Meteorol. Soc. 146 (730), 1999–2049.

Hochman, A., Alpert, P., Harpaz, T., Saaroni, H., Messori, G., 2019. A new dynamical systems perspective on atmospheric predictability: Eastern Mediterranean weather regimes as a case study. Sci. Adv. 5 (6), eaau0936.

Hochman, A., Komacek, T.D., De Luca, P., 2023a. Analogous response of temperate terrestrial exoplanets and earth's climate dynamics to greenhouse gas supplement. Sci. Rep. 13 (1), 11123.

Hochman, A., Messori, G., Quinting, J.F., Pinto, J.G., Grams, C.M., 2021a. Do Atlantic-European weather regimes physically exist? Geophys. Res. Lett. 48 (20), e2021GL095574.

Hochman, A., Plotnik, T., Marra, F., Shehter, E.-R., Raveh-Rubin, S., Magaritz-Ronen, L., 2023b. The sources of extreme precipitation predictability; the case of the 'Wet'Red Sea Trough. Weather. Clim. Extrem. 40, 100564.

Hochman, A., Scher, S., Quinting, J., Pinto, J.G., Messori, G., 2021b. A new view of heat wave dynamics and predictability over the eastern mediterranean. Earth Syst. Dyn. 12 (1), 133–149.

Hochman, A., Scher, S., Quinting, J., Pinto, J.G., Messori, G., 2022. Dynamics and predictability of cold spells over the eastern mediterranean. Clim. Dyn. 58 (7), 2047–2064.

Hoskins, B.J., McIntyre, M.E., Robertson, A.W., 1985. On the use and significance of isentropic potential vorticity maps. Q. J. R. Meteorol. Soc. 111 (470), 877–946.

Hoy, A., Schucknecht, A., Sepp, M., Matschullat, J., 2014. Large-scale synoptic types and their impact on European precipitation. Theor. Appl. Climatol. 116, 19–35.

Huang, H., Patricola, C.M., Bercos-Hickey, E., Zhou, Y., Rhoades, A., Risser, M.D., Collins, W.D., 2021. Sources of subseasonal-to-seasonal predictability of atmospheric rivers and precipitation in the western United States. J. Geophys. Res.: Atmospheres 126 (6), e2020JD034053.

IPMA, 2023. Boletim Portugal dezembro 2022 continental. URL https://www.ipma.pt/pt/media/noticias/documentos/2022/Boletim_clima_IPMA_dez2022.pdf.

Lavers, D.A., Pappenberger, F., Richardson, D.S., Zsoter, E., 2016. ECMWF extreme forecast index for water vapor transport: A forecast tool for atmospheric rivers and extreme precipitation. Geophys. Res. Lett. 43 (22), 11–852.

Lavers, D.A., Ralph, F.M., Richardson, D.S., Pappenberger, F., 2020. Improved forecasts of atmospheric rivers through systematic reconnaissance, better modelling, and insights on conversion of rain to flooding. Commun. Earth & Environ. 1 (1), 39.

Lavers, D.A., Villarini, G., 2013. The nexus between atmospheric rivers and extreme precipitation across europe. Geophys. Res. Lett. 40 (12), 3259–3264.

Lavers, D.A., Villarini, G., Allan, R.P., Wood, E.F., Wade, A.J., 2012. The detection of atmospheric rivers in atmospheric reanalyses and their links to british winter floods and the large-scale climatic circulation. J. Geophys. Res.: Atmospheres 117 (D20).

Lembo, V., Bordoni, S., Bevacqua, E., Domeisen, D.I., Franzke, C.L., Galfi, V.M., Garfinkel, C., Grams, C.I., Hochman, A., Jha, R., et al., 2024. Dynamics, statistics and predictability of rossby waves, heatwaves and spatially compounded extreme events. Bull. Am. Meteorol. Soc..

Liberato, M.L., Pinto, J.G., Trigo, I.F., Trigo, R.M., 2011. Klaus–an exceptional winter storm over northern iberia and southern France. Weather 66 (12), 330–334.

Lorenz, E.N., 1963. Deterministic nonperiodic flow. J. Atmospheres Sci. 20 (2), 130–141.

Lucarini, V., Faranda, D., de Freitas, J.M.M., Holland, M., Kuna, T., Nicol, M., Todd, M., Vaienti, S., et al., 2016. Extremes and Recurrence in Dynamical Systems. John Wiley & Sons.

Ma, W., Chen, G., Guan, B., Shields, C.A., Tian, B., Yanez, E., 2023. Evaluating the representations of atmospheric rivers and their associated precipitation in reanalyses with satellite observations. J. Geophys. Res.: Atmospheres 128 (22), e2023JD038937.

Mariotti, A., Baggett, C., Barnes, E.A., Becker, E., Butler, A., Collins, D.C., Dirmeyer, P.A., Ferranti, L., Johnson, N.C., Jones, J., et al., 2020. Windows of opportunity for skillful forecasts subseasonal to seasonal and beyond. Bull. Am. Meteorol. Soc. 101 (5), E608–E625.

Merz, B., Kuhlicke, C., Kunz, M., Pittore, M., Babeyko, A., Bresch, D.N., Domeisen, D.I., Feser, F., Koszalka, I., Kreibich, H., et al., 2020. Impact forecasting to support emergency management of natural hazards. Rev. Geophys. 58 (4), e2020RG000704.

Messori, G., Caballero, R., Faranda, D., 2017. A dynamical systems approach to studying midlatitude weather extremes. Geophys. Res. Lett. 44 (7), 3346–3354.

Michaelides, S., Karacostas, T., Sánchez, J.L., Retalis, A., Pytharoulis, I., Homar, V., Romero, R., Zanis, P., Giannakopoulos, C., Bühl, J., et al., 2018. Reviews and perspectives of high impact atmospheric processes in the Mediterranean. Atmos. Res. 208, 4–44.

Pereira, S., Ramos, A., Rebelo, L., Trigo, R., Zêzere, J., 2018. A centennial catalogue of hydro-geomorphological events and their atmospheric forcing. Adv. Water Resour. 122, 98–112.

Ralph, F.M., Rutz, J.J., Cordeira, J.M., Dettinger, M., Anderson, M., Reynolds, D., Schick, L.J., Smallcomb, C., 2019. A scale to characterize the strength and impacts of atmospheric rivers. Bull. Am. Meteorol. Soc. 100 (2), 269–289.

Ramos, A.M., Cortesi, N., Trigo, R.M., 2014a. Circulation weather types and spatial variability of daily precipitation in the Iberian Peninsula. Front. Earth Sci. 2, 25.

Ramos, A.M., Martins, M.J., Tomé, R., Trigo, R.M., 2018. Extreme precipitation events in summer in the Iberian Peninsula and its relationship with atmospheric rivers. Front. Earth Sci. 6, 110.

Ramos, A.M., Nieto, R., Tomé, R., Gimeno, L., Trigo, R., Liberato, M., Lavers, D., 2016a. Atmospheric rivers moisture sources from a lagrangian perspective. Earth Syst. Dynam. 7, 371–384.

Ramos, A.M., Roca, R., Soares, P.M., Wilson, A.M., Trigo, R.M., Ralph, F.M., 2021. Uncertainty in different precipitation products in the case of two atmospheric river events. Environ. Res. Lett. 16 (4), 045012.

Ramos, A.M., Sousa, P.M., Dutra, E., Trigo, R.M., 2020. Predictive skill for atmospheric rivers in the western Iberian Peninsula. Nat. Hazards Earth Syst. Sci. 20 (3), 877–888.

Ramos, A.M., Tomé, R., Trigo, R.M., Liberato, M.L., Pinto, J.G., 2016b. Projected changes in atmospheric rivers affecting europe in cmip5 models. Geophys. Res. Lett. 43 (17), 9315–9323.

Ramos, A.M., Trigo, R.M., Liberato, M.L., 2014b. A ranking of high-resolution daily precipitation extreme events for the Iberian Peninsula. Atmospheric Sci. Lett. 15 (4), 328–334.

Ramos, A.M., Trigo, R.M., Liberato, M.L., Tomé, R., 2015. Daily precipitation extreme events in the Iberian Peninsula and its association with atmospheric rivers. J. Hydrometeorol. 16 (2), 579–597.

Ribeiro, S.L., Gonçalves, A., Cascarejo, I., Liberato, M.L.R., Fonseca, T.F., 2022. Development of a catalogue of damage in portuguese forest associated with extreme extratropical cyclones. Sci. Total Environ. (ISSN: 0048-9697) 814, 151948. http://dx.doi.org/10.1016/j.scitotenv.2021.151948, URL https://www.sciencedirect.com/science/article/pii/S0048969721070248.

Rutz, J.J., Shields, C.A., Lora, J.M., Payne, A.E., Guan, B., Ullrich, P., O'Brien, T., Leung, L.R., Ralph, F.M., Wehner, M., Brands, S., Collow, A., Goldenson, N., Gorodetskaya, I., Griffith, H., Kashinath, K., Kawzenuk, B., Krishnan, H., Kurlin, V., Lavers, D., Magnusdottir, G., Mahoney, K., McClenny, E., Muszynski, G., Nguyen, P.D., Prabhat, M., Qian, Y., Ramos, A.M., Sarangi, C., Sellars, S., Shulgina, T., Tome, R., Waliser, D., Walton, D., Wick, G., Wilson, A.M., Viale, M., 2019. The atmospheric river tracking method intercomparison project (ARTMIP): Quantifying uncertainties in atmospheric river climatology. J. Geophys. Res.: Atmospheres 124 (24), 13777–13802. http://dx.doi.org/10.1029/2019JD030936, URL https://agupubs.onlinelibrary.wiley.com/doi/abs/10.1029/2019JD030936.

Santos, M., Fonseca, A., Fragoso, M., Santos, J.A., 2019. Recent and future changes of precipitation extremes in mainland Portugal. Theor. Appl. Climatol. 137 (1), 1305–1319.

Seneviratne, S.I., Zhang, X., Adnan, M., Badi, W., Dereczynski, C., Di Luca, A., Ghosh, S., Iskandar, I., Kossin, J., Lewis, S., Otto, F., Pinto, I., Satoh, M., Vicente-Serrano, S.M., Wehner, M., Zhou, B., 2021. Weather and climate extreme events in a changing climate. In: Masson-Delmotte, V., Zhai, P., Pirani, A., Connors, S.L., Péan, C., Berger, S., Caud, N., Chen, Y., Goldfarb, L., Gomis, M.I., Huang, M., Leitzell, K., Lonnoy, E., Matthews, J.B.R., Maycock, T.K., Waterfield, T., ci, O.Y., Yu, R., Zhou, B. (Eds.), Climate Change 2021: The Physical Science Basis. Contribution of Working Group I To the Sixth Assessment Report of the Intergovernmental Panel on Climate Change. Cambridge University Press, Cambridge, United Kingdom and New York, NY, USA, pp. 1513–1766. http://dx.doi.org/10.1017/9781009157896.013.

Sillmann, J., Thorarinsdottir, T., Keenlyside, N., Schaller, N., Alexander, L.V., Hegerl, G., Seneviratne, S.I., Vautard, R., Zhang, X., Zwiers, F.W., 2017. Understanding, modeling and predicting weather and climate extremes: Challenges and opportunities. Weather. Clim. Extrem. 18, 65–74.

Slingo, J., Palmer, T., 2011. Uncertainty in weather and climate prediction. Philos. Trans. R. Soc. A: Math. Phys. Eng. Sci. 369 (1956), 4751–4767.

Süveges, M., 2007. Likelihood estimation of the extremal index. Extremes 10 (1), 41–55.

Vakrat, E., Hochman, A., 2023. Dynamical systems insights on cyclonic compound "wet" and "windy" extremes in the eastern mediterranean. Q. J. R. Meteorol. Soc. 149 (757), 3593–3606.

Zhou, Y., Kim, H., Guan, B., 2018. Life cycle of atmospheric rivers: Identification and climatological characteristics. J. Geophys. Res.: Atmospheres 123 (22), 12–715.